Energy transfer in Er-doped SiO_2 sensitized with Si nanocrystals

I. Izeddin,* D. Timmerman, and T. Gregorkiewicz
Van der Waals-Zeeman Institute, University of Amsterdam, Valckenierstraat 65, NL-1018XE Amsterdam, The Netherlands

A. S. Moskalenko
Institut für Physik, Martin-Luther-Universität Halle-Wittenberg, Nanotechnikum-Weinberg, Heinrich-Damerow-St. 4, 06120 Halle, Germany

A. A. Prokofiev and I. N. Yassievich
Ioffe Physico-Technical Institute, Russian Academy of Sciences, Politekhnicheskaya 26, 194021 St. Petersburg, Russia

M. Fujii
Department of Electrical and Electronic Engineering, Faculty of Engineering, Kobe University, Rokkodai, Nada, Kobe 657-8501, Japan

(Received 18 February 2008; revised manuscript received 9 May 2008; published 23 July 2008)

We present a high-resolution photoluminescence study of Er-doped SiO_2 sensitized with Si nanocrystals (Si NCs). Emission bands originating from recombination of excitons confined in Si NCs, internal transitions within the $4f$-electron core of Er^{3+} ions, and a band centered at $\lambda \approx 1200$ nm have been identified. Their kinetics were investigated in detail. Based on these measurements, we present a comprehensive model for energy-transfer mechanisms responsible for light generation in this system. A unique picture of energy flow between the two subsystems was developed, yielding truly microscopic information on the sensitization effect and its limitations. In particular, we show that most of the Er^{3+} ions available in the system are participating in the energy exchange. The long-standing problem of apparent loss of optical activity in the majority of Er dopants upon sensitization with Si NCs is clarified and assigned to the appearance of a very efficient energy exchange mechanism between Si NCs and Er^{3+} ions. Application potential of SiO_2:Er, sensitized by Si NCs, was discussed in view of the newly acquired microscopic insight.

DOI: 10.1103/PhysRevB.78.035327 PACS number(s): 78.55.−m, 31.70.Hq, 78.67.Bf, 73.21.La

I. INTRODUCTION

SiO_2 matrix doped with Er^{3+} ions and Si nanocrystals (Si NCs) is intensively investigated as an interesting system where room temperature 1.5 μm Er-related emission can efficiently be induced by nonresonant excitation. Some time ago it has been noted that photoluminescence and electroluminescence of Er^{3+} ions in SiO_2 can be effectively sensitized with Si quantum dots.[1–5] In photoluminescence, upon illumination, incoming photons are predominantly absorbed by band-to-band transitions in Si NCs. Since the indirect band structure of Si is preserved also in the nanocrystalline form,[6] electron-hole pairs generated in this way are characterized by a relatively long lifetime. This enables energy transfer to Er^{3+} ions located in vicinity of Si NCs. In that way, a channel of indirect excitation of Er dispersed in SiO_2 is created and the 1.5 μm Er-related emission appears. Its temporal characteristics comprises a microsecond rise time, corresponding to Si-NC-to-Er energy transfer, followed by predominantly radiative and temperature-independent decay in the millisecond range, characteristic for Er^{3+} ions in SiO_2. It has been concluded that dispersion of Si nanocrystals in Er-doped SiO_2 matrix SiO_2:(Er, Si NCs) combines, to a certain extent, positive features of Er-doped crystalline Si with those of Er-doped SiO_2: (i) In contrast to the situation for SiO_2:Er, introduction of Si NCs enables indirect excitation of Er^{3+} ions. This process is nonresonant and relatively efficient with an (effective) excitation cross section of $\sigma \approx 10^{-17}-10^{-16}$ cm^{-2}, which represents an increase by a factor of 10^3 (Ref. 4) in comparison to SiO_2:Er. (ii) In contrast to the situation in crystalline Si:Er, emission from Er^{3+} ions does not suffer from thermal quenching and is readily observed at room temperature, similar to SiO_2:Er.[4,5]

These promising characteristics raised considerable hopes on possible applications of the SiO_2:(Er, Si NCs) for Si photonics and specific devices have been proposed.[7–9] Particularly attractive is the prospect application of SiO_2:(Er, Si NCs) for development of a flash-lamp pumped optical amplifier—a much welcome replacement for the currently used fiber amplifier, which requires resonant and high power laser pumps for its operation. In order to achieve that, the Si-NC-induced sensitization process of Er emission in SiO_2 has to be thoroughly understood.

In the past, Förster (dipole-dipole) mechanism[10] has been proposed in order to explain the energy transfer from Si NCs to Er^{3+} (Refs. 11 and 12) and different locations of Er, with respect to Si NC, have been considered.[13,14] In addition to the relatively slow (μs range) NC-mediated Er^{3+} excitation, a much faster (100 ns range) and usually more dominating process has also been concluded.[15] Its physical origin has been considered recently[16] and participation of special luminescence centers in erbium excitation has been postulated in particular for low-temperature annealed samples. However, in spite of a considerable progress by both modeling and experiment,[4,17] many issues still lack sufficient explanation. In this field, while reports on optical gain have been published,[18] detailed investigations revealed important drawbacks of the SiO_2:(Er, Si NCs) system: it has been realized

that (i) only a relatively small part of all the Er^{3+} ions is susceptible to the indirect excitation via Si NCs,[19,20] and (ii) upon introduction of Si NCs, a considerable portion of Er dopants loses so-called "optical activity" and does not contribute photons regardless of the excitation mode (via Si NCs or directly by resonant pumping).[19] Therefore it has become clear that dispersion of Si NCs in SiO_2:Er is a challenging and complex physical system, which has to be understood, and possibly engineered at a microscopic level, before device applications can be considered.

In our previous contribution,[21] submicrosecond Er-related luminescence from the SiO_2:(Er, Si NCs) system was reported, and an Auger-facilitated energy-transfer process between carriers within the quantized levels of the NCs and Er^{3+} was proposed as the excitation and deexcitation mechanism. It was also shown that up to ~50% of the total Er content is involved in this process and contributes to the sub-μs emission. In this paper, we study, in depth, temporal details of emission bands from SiO_2:(Er, Si NCs). Using optical excitation with nanosecond pulses and time-correlated photon-counting detection mode, we resolve true kinetics of emissions related to Si NCs and Er^{3+} ions present in the investigated material. Based on this information, we propose a complete microscopic scenario of energy-transfer processes in the SiO_2:(Er, Si NCs) system. The chosen approach allows us to identify emissions from most of the Er dopants available in the material. Using a theoretical model, we discuss microscopic aspects of energy-transfer processes between Si NCs and Er^{3+} ions in relation to their (mutual) location in the SiO_2 matrix.

II. EXPERIMENT

For the purpose of this study, a series of Si-NC- and Er-doped SiO_2 2 μm layers were prepared by radio frequency cosputtering on a SiO_2 substrate. The samples were characterized by different concentrations of Er dopants, and size and concentration of Si NCs. Details of sample preparation procedure can be found in Ref. 2. Following preliminary selection, the detailed investigation of recombination dynamics has been conducted on a particular sample with the most intense 1.5 μm Er-related emission. It was characterized by atomic concentrations of 0.11% of Er, 41.8% of Si, and 12.6% of excess Si. After the sputtering procedure, the sample underwent annealing at 1100 °C, which resulted in formation of Si NCs with an average diameter of 3.1 nm, a size dispersion of ≈14%, and a density (for NC) of ≈4.1 $\times 10^{18}$ cm^{-3}. A twin sample without Er dopant but with the same concentration and size of Si NCs was used for the absorption measurements.

The photoluminescence (PL) experiments were performed under pulsed excitation in the visible range, provided by a tunable optical parametric oscillator (OPO) pumped by the third harmonic of a Nd: yttrium aluminum garnet (YAG) laser with pulse duration of 5 ns and repetition rate of 10 Hz. In the UV range experiments, the excitation was provided by the third harmonic of a Nd:YAG. The samples were placed on a cold finger of closed-cycle cryostat, and the measurements were taken at 10 K and room temperature (RT). PL spectra were resolved with a TRIAX 320 spectrometer and detected with an InGaAs photomultiplier tube (PMT) with flat response in the visible to near-infrared range or a Ge photodiode (Edinburgh Instruments EI-A) connected to a digital oscilloscope where signal integration was done. For time-resolved measurements of PL dynamics, the PMT was working in time-correlated photon-counting mode with temporal resolution up to 2 ns.

The absorption measurements were performed in two experimental configurations: Direct transmission measurements under OPO pulsed illumination and in a UV absorption photospectrometer.

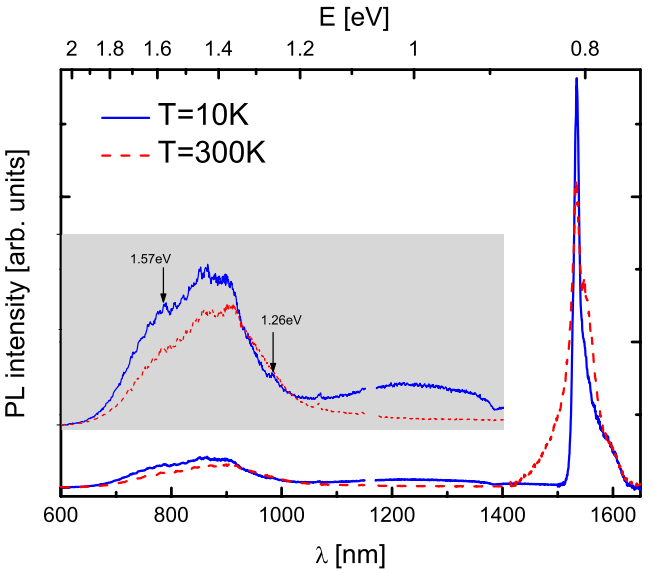

FIG. 1. (Color online) Time-integrated PL spectra at $T=10$ and 300 K, and excitation wavelength $\lambda_{exc}=450$ nm. Si-NC-related, Er-related, and a third (at low T) PL bands can be observed. The Si-NC-related band is blown up for clarity. The arrows show PL peaks related to emission from higher excited states of the Er^{3+} ion, superimposed to the NC excitonic PL.

III. RESULTS

A. Photoluminescence spectra

Figure 1 shows the PL spectra of the investigated sample at RT and at 10 K. The measurements were performed under pulsed excitation at $\lambda=450$ nm (2.75 eV), i.e., not in resonance with any internal transition of Er. The total time-integrated PL response of the sample is given, which reflects the number of photons emitted. Both, Er- and Si-NC-related PL bands are observed simultaneously with their mutual intensity ratio determined by the Er concentration, which is in agreement with earlier studies.[2] In addition, at low temperature, a weaker band centered at $\lambda \approx 1200$ nm can be seen: it has a short decay time constant and therefore its time-integrated intensity is small compared to the other two bands.

We note that the Er-related emission band broadens at RT, keeping its wavelength integrated intensity practically constant, which is also in concordance with previous reports.

The broadening at RT is produced mainly in the higher energy side of the spectrum, and the full width at half maximum (FWHM) increases from ≈6.7 to ≈20 meV at 10 K and RT, respectively. This could be due to population of upper states of the multiplet $^4I_{13/2}$ by thermalization.

The Si NCs show a broad excitonic-related PL band. If we take into account the NCs size (radius $R=1.55$ nm) and dispersion (≈14%), the position and width of the excitonic-related PL band can be estimated on the basis of the calculated band gap of the NCs as a function of their size.[22] The emission energy is given by $E=E_g^{Si}+E_{1e}+E_{1h}-E_{\text{excit}}-\hbar\omega \approx 1.5$ eV (with E_g^{Si} corresponding to the energy-band gap of crystalline silicon, E_{1e}, E_{1h}, and E_{excit} are the electron and hole level quantization corrections, and the excitonic correction, respectively—taken from Ref. 22—and the phonon energy $\hbar\omega=60$ meV), i.e., a band centered at 850 nm, ranging from ≈820 to ≈870 nm, taking into account their size dispersion. Comparison with experiment shows that the center of the band is in very good agreement with the expected value but the experimentally recorded band is broader than expected from the calculations with the higher energy side of the band suffering from strong temperature quenching. Since optical excitation was provided by short-wavelength photons of 450 nm (2.75 eV), thus creating "hot" carriers in the higher energy states of the Si NCs, then it is reasonable to consider the origin of the higher energy side of the NC-related PL band as arising from hot carriers in the upper electron (and/or hole) levels of the Si NCs.

Superimposed on the Si NCs PL band recorded at 10 K, peaks with positions at 1.26 and 1.57 eV are observed. These correspond to emissions from the second-excited and the third-excited states of Er, and disappear at room temperature. We note that in view of the exclusively nonresonant excitation mode, the observation of these peaks indicates that the Er^{3+} excitation proceeds, at least partly, via higher excited states.

The effective lifetime of the excited state of Er in SiO_2 with Si NCs lies within 2–3 ms. Decay of excitons in Si NCs is governed by a stretched exponential function, with a long final tail, with decay time constant of 20–50 μs, as will be shown later. The decay of the band centered at λ ≈1200 nm is clearly faster, being predominantly nonradiative; the lifetime shortens further at a higher temperature, leading to a strong reduction in the time-integrated PL intensity of this band at RT.

B. High-resolution photoluminescence kinetics

Using the time-correlated photon-counting technique to resolve the time evolution of the PL transient revealed new insight into excitation and deexcitation dynamics in the SiO_2:(Er, Si NCs) system.[21] This experimental technique allows for simultaneous recording of very different dynamical ranges without suffering from signal distortion. Panel **a** in Fig. 2 presents a time-resolved PL spectrum of the excitonic PL band from Si NCs. The contour plot shows how the peak of maximum intensity drifts to longer wavelengths, i.e., lower energy, at longer delays. Consequently, the PL decay constant of the luminescence increases for longer wavelengths. This is understandable when we consider the NC size distribution: excitonic PL dynamics in smaller NCs is faster than in larger quantum dots. In the Si NCs under consideration, the phonon-assisted radiative transition dominates over the direct radiative transition. The probability of such a transition increases rapidly with the decrease in the NC size (see Ref. 22). In panel **b** of Fig. 2, the time-resolved PL spectrum of Si NCs is shown in the submicrosecond time range; we can observe the center of the band at λ=775 nm (1.6 eV), in contrast to the previous figure. If we compare the spectra measured at 100 ns and at 100 μs after the excitation pulse, a difference of ≈200 meV separates the centers of the two bands. We can assign the submicrosecond PL to recombination of carriers from the higher Si-NC states.

Figure 3 shows measurements related to the broad PL band appearing in the spectral range between the NC- and Er-related emissions. In the inset, the spectrum recorded at 200 ns after the excitation pulse and at $T=10$ K, shows the broad band centered at λ≈1200 nm. The lifetime of this PL band, as mentioned before, shortens at higher temperatures, becoming practically negligible at RT. This can be seen in the main panel, where the RT PL transient kinetics recorded at the maximum of the band (1200 nm) is compared to the PL at 1535 nm. One can see that after 100 ns, the decay of the PL at 1535 nm can be attributed to the Er-related PL. The origin of the band centered at λ≈1200 nm is usually identified as recombination at defects but its broadness and fast kinetics seem to contradict this identification; future investigations—out of the scope of this paper—will elucidate this point.

In Fig. 4, the high-resolution kinetics of the excitonic luminescence from Si NCs can be followed in panel **a**. An intense PL signal with a fast decay, also characterized in the submicrosecond time domain, is observed after the excitation pulse. This is stretched until the final slower tale—of the order of 30–50 μs—is achieved, as shown in Fig. 2. Panel **b** of the same figure shows the Er-related PL kinetics for the first microsecond after the excitation pulse, at $T=10$ K and RT.

In our previous contribution,[21] we have analyzed detailed kinetics of Er-related PL sensitized by Si NC and have shown that it exhibits three separate regimes. Regime I—for $t \leq 1$ μs: a strong emission appears, immediately following the laser pulse and then rapidly decays toward a temporary minimum. Regime II—for $1\ \mu s \leq t \leq 10\ \mu s$: Er-related PL intensity rises slowly again and reaches a broad maximum whose amplitude is at least an order of magnitude smaller than the initial value in Regime I. Regime III—for $t > 10$ μs: PL intensity slowly decays with a millisecond time constant. We have also shown that the microsecond rise of the Er-related PL in regime II ($\tau_{\text{Er}}^{\text{rise}} \approx 3.5$ μs) is paralleled by a decay of Si-NC PL, which can be characterized by a stretched exponent with $\tau_{\text{NC}} \approx 1.2$ μs, illustrating in this way the relatively slow energy transfer between Si-NCs and Er^{3+} ions. This decay of NC-related PL slows down once Er emission attains a maximum. At this stage the NC-mediated excitation of Er is completed or saturated[19] and therefore further decay of the NC-related PL is decoupled from Er. Careful inspection revealed that the local minimum of Er PL intensity from which the "slow" rise begins is equal to ap-

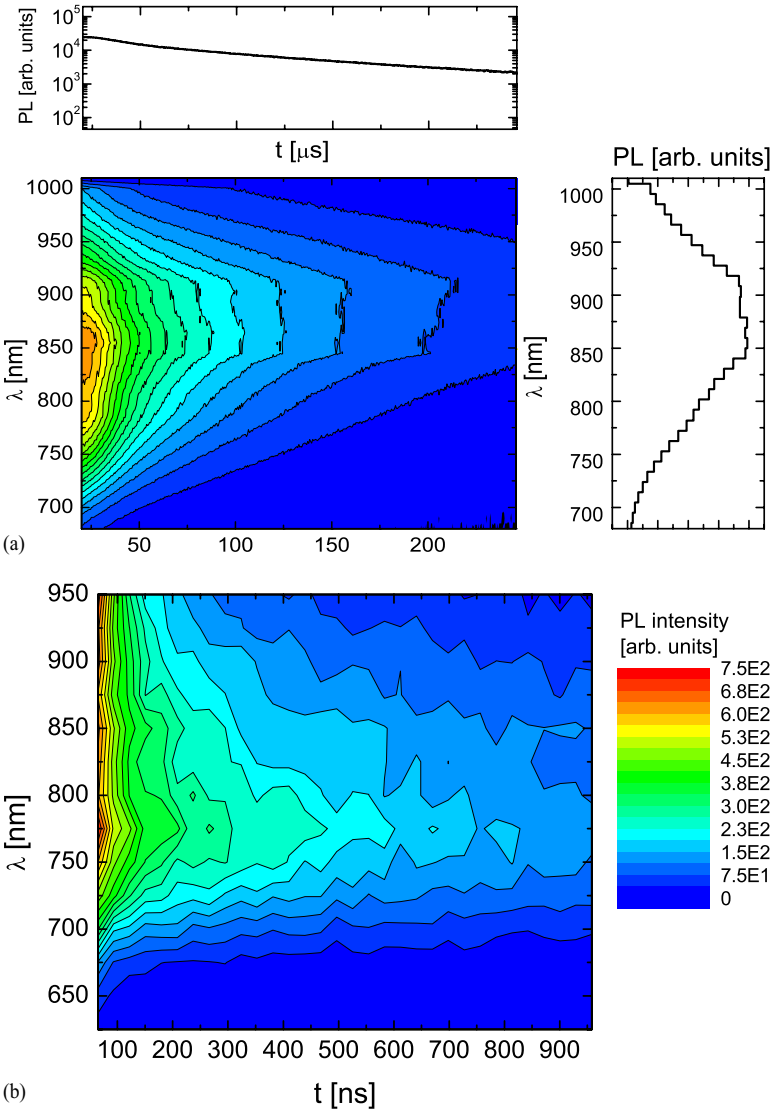

FIG. 2. (Color online) Time-resolved contour plot of the PL spectrum of the Si-NC excitonic-related band in the (a) microseconds and in the (b) submicrosecond time ranges. The PL intensity (colored contour plots) is represented as a function of time (X axis) and detection wavelength (Y axis). Panel (a) also shows the spectrum recorded at $t=100$ μs and the PL decay at $\lambda=850$ nm (sections from the contour plot). Drift of the band maximum toward longer wavelength is observed for longer time delay in panel (a). Note the difference between the center of the bands in both figures (≈ 200 meV).

proximately half of the maximum intensity attained in regime II. We recall that such an initial amplitude of Er PL attained very shortly after excitation (regime I) was also reported before.[23] Based on the total evaluation of optically active Er fraction, we conclude that the "residual concentration" of Er^{3+} ions involved in the slow excitation/slow recombination process (regimes II and III) amounts to $\sim 0.2\%$ of the total Er content.

To validate the idea of hot carriers in the Si NCs being responsible for the submicrosecond Er-related luminescence postulated in our previous contribution,[21] we investigate the intensity ratio between the fast and the slow components of Er PL for different excitation wavelengths and fluxes. Both fast (submicrosecond) and slow (milliseconds) components of the Er-related transient PL must be governed by different excitation and deexcitation mechanisms. The intensity ratio of these components is thus likely to depend on the excitation conditions. Figure 5 shows full, high-resolution kinetics of Er^{3+} PL under different excitation wavelengths and powers, normalized for the maximum intensity of the slow component. One can observe a higher fast-to-slow intensity ratio when higher power or larger photon energy quantum is used for excitation.

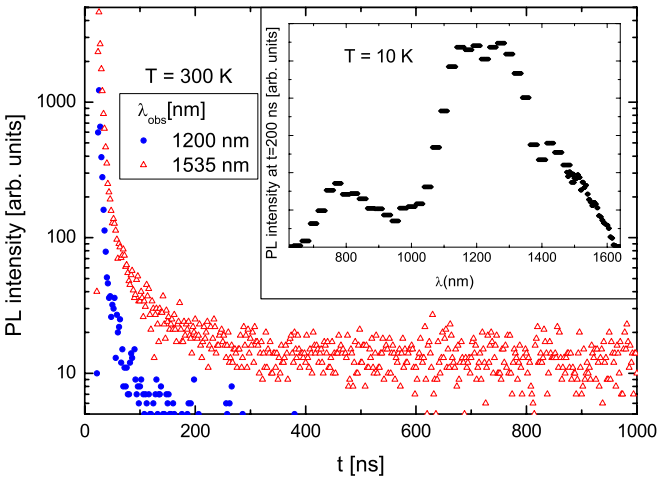

FIG. 3. (Color online) Room temperature PL decay kinetics recorded at $\lambda=1200$ nm (maximum of the PL broad band shown in Fig. 1) and $\lambda=1535$ nm. In the inset, the spectrum recorded at $t=200$ ns after the laser excitation pulse, at $T=10$ K, is shown.

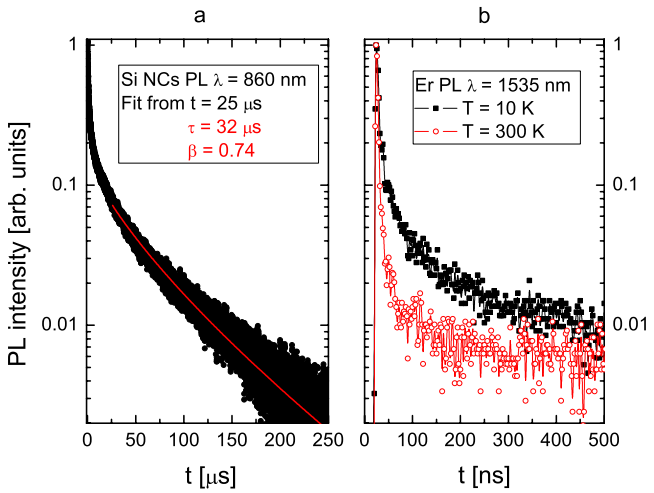

FIG. 4. (Color online) In panel a: Si-NC PL kinetics, recorded at $\lambda = 860$ nm and room temperature; time resolution of the system was 2 ns. Excitation was provided with a 5 ns pulse at $\lambda_{exc} = 450$ nm. Initial nanoseconds decay is stretched and followed by a final decay with characteristic lifetime of thick microseconds. In panel b: Er-related 1.5 μm PL kinetics for the first microsecond after the excitation pulse is shown at $T = 10$ K and RT.

C. Excitation cross-section measurements

The excitation cross section of Si NCs and Er PL, σ_{NC} and σ_{Er}, respectively, is of crucial importance to understand the excitation processes, and energy transfer between Si NCs and Er^{3+} ions. In order to gain insight into this aspect, flux dependencies of Si NC- and Er-related PL signals were recorded; a reference sample without Er doping was used for the NC-related PL measurements. In Fig. 6, PL flux dependencies for different excitation wavelengths are shown, recorded at 1535 and 912 nm, for the Er-doped and Er-free samples, respectively. The curves have been fitted to the excitation dependence of PL intensity, derived from the rate equations for pulsed excitation,

$$I_{PL} \propto N^* = N(1 - e^{-\sigma\phi\Delta t}), \quad (1)$$

where I_{PL} is the time-integrated PL intensity in arbitrary units, N^* is the number (concentration) of excited emitters (Er^{3+} ions or Si NCs), N is the total number (concentration) of excitable Er^{3+} ions or NCs, σ is the effective excitation cross section, ϕ is the photon flux of excitation, and Δt the laser-pulse duration. Remark that formula (1) is valid only in a limit of one radiative exciton per Si NC.[19] The effective excitation cross section σ is determined from the experimentally measured dependencies depicted in Fig. 6 by fitting them using formula (1). The resulting values for both Si NCs and Er luminescence (σ_{NC} and σ_{Er}) are shown in Fig. 7 as a function of the excitation wavelength.

Directly related to the effective PL excitation cross section σ_{PL}, we studied the optical-absorption coefficient in our SiO_2:Si NCs reference sample. The effective (Er- and NC-related) PL excitation cross-section values (Fig. 7) are plotted in Fig. 8 as a function of the measured Si NCs' absorption coefficient α for each given excitation wavelength λ_{exc}. A linear relation between absorption and excitation can be observed in all the investigated range for Si-NCs; in the case of Er-related luminescence, a change of linear relation is observed at an energy threshold, i.e., at ~2.6–2.7 eV (≈460–470 nm), an energy above which the excitation cross section grows faster than the absorption.

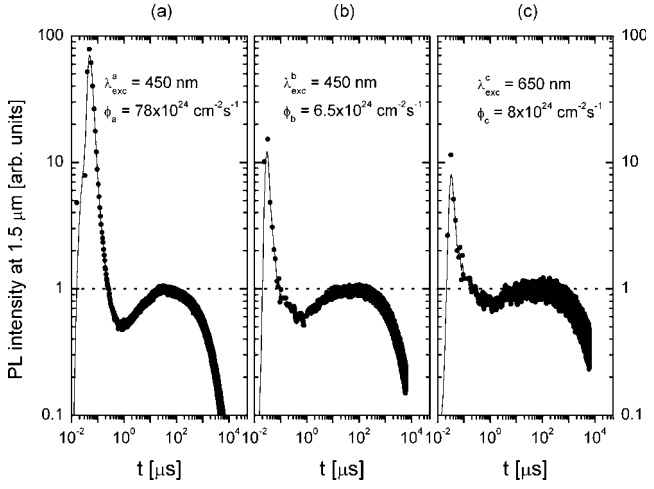

FIG. 5. Er-related PL kinetics in double-logarithmic scale for different excitation conditions at RT. Intensity has been normalized to the maximum of the slow component in order to compare the fast-to-slow intensity ratio. In panels (a) and (b), the excitation wavelength (450 nm) has been kept constant and flux has been decreased about one order of magnitude. In panels (b) and (c), flux has been kept in the same order of magnitude and wavelength excitation has been increased to 650 nm.

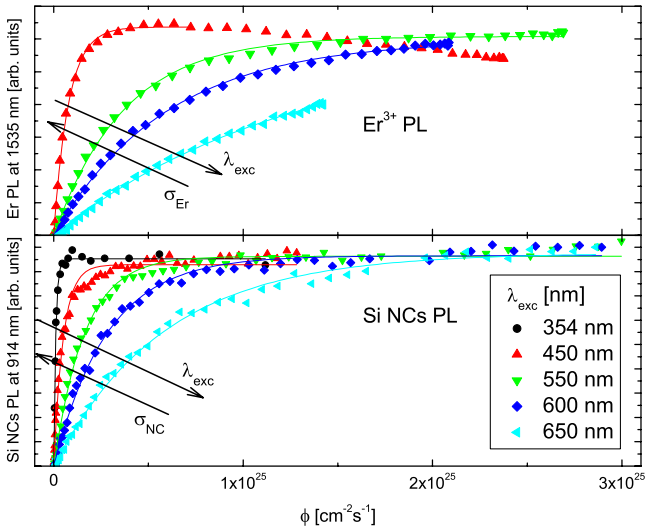

FIG. 6. (Color online) Flux dependence of Er^{3+} and Si-NC PL for several excitation wavelengths is shown, recorded at RT.

IV. THEORY

In order to rationalize the experimental results gathered in this study, we consider the possible processes of energy exchange between carriers confined in Si NCs and Er^{3+} ions in SiO_2 (outside NC).

Energy transfer between electrons and holes in NCs and f electrons of Er^{3+} ion is implemented as an Auger process

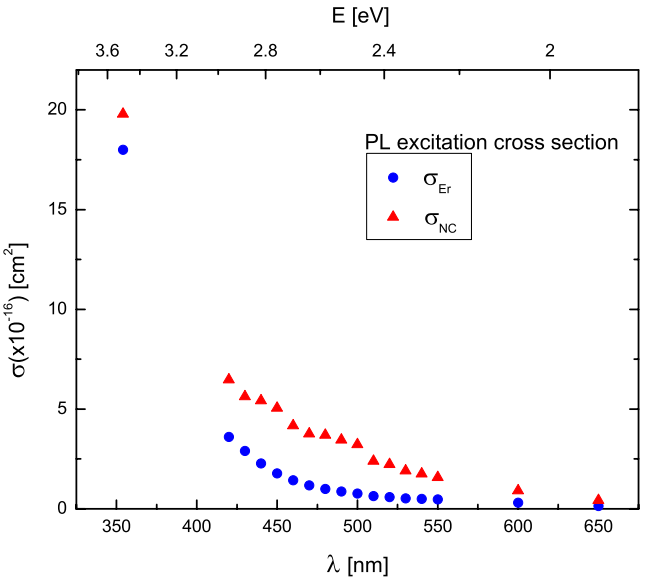

FIG. 7. (Color online) PL excitation cross section of Er^{3+} and Si-NC PL as a function of excitation wavelength, which have been determined by using formula (1) to fit the curves of Fig. 6.

(i.e., via the Coulomb interaction).The energy can be transferred to an erbium ion either when a confined electron-hole pair recombines or when an intraband transition of confined carrier occurs. Both processes can be accompanied by multiphonon transitions to fulfill the energy conservation law as the energy spectra of both electron systems are discrete. The momentum conservation law plays an important role in the Auger recombination processes as the large momentum should be transferred by the electron-hole recombination due to the indirect band structure of silicon.

Confined electron and hole energy levels as well as their wave functions calculated in multiband effective-mass approximation[22] are used in this consideration. Luttinger Hamiltonian in the spherical approximation has been used

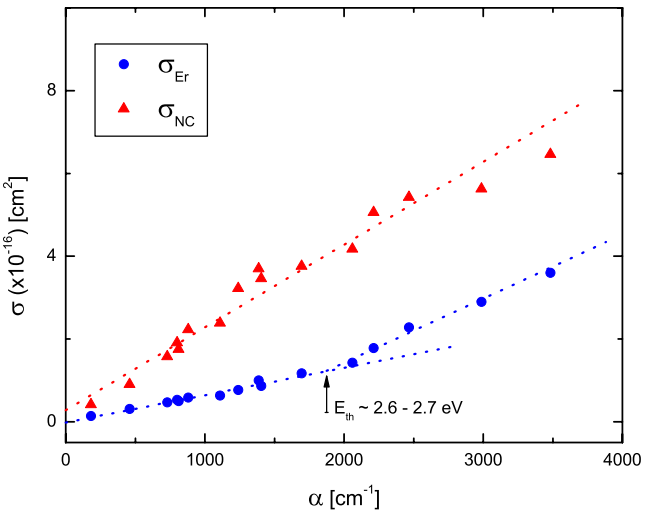

FIG. 8. (Color online) Er- and Si-NC-related effective excitation cross section σ_{PL} as a function of the optical-absorption coefficient α for each given excitation wavelength.

for holes and the strong anisotropy of the electron effective mass in silicon has been taken into account. The wave function and flux continuities were used as the boundary conditions.[24,25] When calculating wave functions outside the NC, isotropic effective masses being equal to m_0 and $5m_0$ were used for electron and hole states correspondingly. Spin-orbit splitting was neglected in both Si and SiO_2.

The conduction band of Si has six equivalent minima in the first Brillouin zone, situated in the neighborhoods of the six X points. The wave function of electron can be presented in the form:

$$\psi_\nu^e = \xi^e(\mathbf{r}) u_{c\nu} \exp(i\mathbf{k}_{0\nu}\mathbf{r}), \tag{2}$$

where $u_{c\nu}$ and $\mathbf{k}_{0\nu}$ ($k_{0\nu}=0.85\times 2\pi/a_{\text{lat}}$) are the Bloch amplitude and wave vector corresponding to the bottom of valley ν ($a_{\text{lat}}=0.54$ nm is the lattice constant of silicon). Envelope functions $\xi^e(\mathbf{r})$ are found as a result of a numerical solution to the Schrödinger equation after separating the angular part $\exp(im\phi)$ (m can be any integer number) as there is a strong anisotropy of the electron effective mass: $m_\parallel=0.916m_0$ and $m_\perp=0.19m_0$. The electron states are sixfold degenerate for $m=0$ and 12 times degenerate for $|m|>0$, as two opposite values $m=\pm|m|$ correspond to the same energy. (This degeneracy is given without taking into account an additional spin degeneracy). So the states are marked with $Ne_{|m|}$ where the letter e shows that it is an electron state and N is the main quantum number that shows the order of the energy level for given $|m|$. For example, the ground state is marked as $1e_0$, which means that this is the first electron state with $m=0$.

The approximation used in Ref. 22 leads to two types of hole states in bulk Si, which correspond to twofold-degenerate heavy-hole band having mass $m_h=0.44m_0$ and nondegenerate light hole band having mass $2m_hm_l/(3m_h-m_l)=0.12m_o$ ($m_l=0.16m_0$ for Si).[26] The quantum confinement gives rise to mixing of the states. There are three types of hole states in spherical quantum dots: (i) mixed states (hm) formed by the combination of heavy and light ones, (ii) heavy-hole (hh) states, and (iii) light hole (hl) states. Each state is also characterized by the full angular momentum F (zero for the light hole states and positive integer for the other ones) and it is $2F+1$ times as degenerate as the projection M of momentum F onto the quantization axis (arbitrary selected), which can be any integer number having absolute value not larger than F. The space quantization forms a series of each type of the states with fixed F. So they are marked with the letters showing the type of the states with index indicating the value of F and the number in a series in front of it all. For example, the hole state with the lowest energy is of the mixed type—$1hm_1$.

The calculated lower energy levels of electrons and holes confined in Si NC of diameter in the range 2.8–3.3 nm are shown in Fig. 9. The energy range is limited to the one of optical pumping used in experiments (2.85 eV). Due to the existence of relatively large energy separations between some neighboring space quantized levels, one phonon emission processes will be suppressed. This effect might lead to the so-called phonon bottleneck slowing down of carrier relaxation. Although in different nanocrystal alternative rapid cooling mechanism have been observed—e.g. CdSe (Ref.

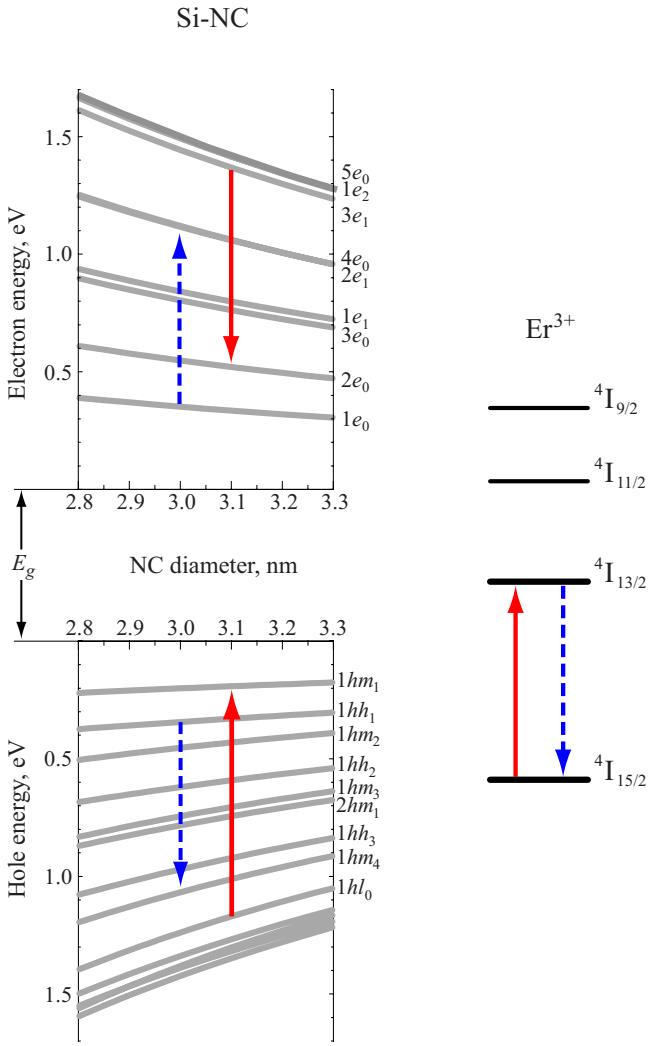

FIG. 9. (Color online) Electron and hole energy levels in Si NCs in SiO_2, as a function of NC diameter. On the right-hand side, the Er^{3+} energy levels are presented. The most effective erbium excitation and deexcitation processes due to intraband carrier transitions are shown.

27)—one can expect that energy relaxation of hot carriers will, in our case, become slower in comparison to bulk silicon. Thus, an Auger excitation of erbium ions in silicon dioxide is possible, similar to the impact ionization by hot carriers in bulk silicon where it plays a significant role in electroluminescence but just negligibly affects the excitation of the erbium photoluminescence due to the fast energy relaxation of hot carriers in the bulk material.

A. Excitation due to intraband transition

The probability of Auger excitation of an erbium ion situated in SiO_2 at the distance a from the center of a Si NC as the result of the transition of a hot confined carrier from the state i into the state i' is given by the Fermi golden rule:

$$W_{i'i} = \frac{2\pi}{\hbar}\frac{1}{N_f}\sum_{ff'} |\langle f', i'|e\Phi|f, i\rangle|^2 J_T(N)\,\delta(E_i - E_{i'} - \Delta_{ff'} - N\hbar\omega_{\mathrm{ph}}), \tag{3}$$

where Φ is the potential created by the f electron of the Er^{3+} ion, f and f' enumerate the states of f electrons of the ion, $\Delta_{ff'}$ is the transition energy, and N_f is the degeneracy degree of the f state. The integration in the matrix elements of Eq. (3) is to be produced over the carriers confinement space and the f-electron coordinate. Due to the energy conservation law, the confined carrier transition is accompanied by the emission of N phonons with energy $\hbar\omega_{\mathrm{ph}}$.

In the Huang-Rhys model (the model of two displaced oscillators with the same frequency), the phonon factor $J_T(N)$ is given by:[28]

$$J_T(N) = \exp\left[-2S\left(N_T + \frac{1}{2}\right)\right] \times \exp\left[\frac{N\hbar\omega_{\mathrm{ph}}}{2kT}\right] I_N[2S\sqrt{N_T(N_T+1)}], \tag{4}$$

where S is the Huang-Rhys factor, which in the one-mode approximation is given by

$$S = \frac{\varepsilon_{\mathrm{opt}} - \varepsilon_{\mathrm{th}}}{\hbar\omega_{\mathrm{ph}}} \tag{5}$$

with $\varepsilon_{\mathrm{opt}}$ and $\varepsilon_{\mathrm{th}}$ corresponding to the optical and thermal ionization energies, respectively, N_T is the Bose-Einstein factor:

$$N_T = \frac{1}{\exp\left(\frac{\hbar\omega_{\mathrm{ph}}}{kT}\right) - 1}, \tag{6}$$

and $I_N(x)$ is the modified Bessel function of order N.

As the energy levels are highly degenerate, one should average over all the initial states with the energy E_i and sum over all the final states corresponding to the energy E_i' in Eq. (3). All these states are actually split due to nonsphericity of NCs and other factors. This fact is taken into account by assuming the broadening of levels and adding the value δE to the argument of δ function in Eq. (3), and averaging over this value in the energy range Δ_E=60 meV (we have assumed that it is about the energy of an optical phonon in bulk Si). As a result Eq. (3) transforms into

$$W_{i'i} = \frac{2\pi}{\hbar}\frac{1}{\Delta_E}\frac{1}{N_i}\sum_{M,M'}\frac{1}{N_f}\sum_{ff'} |\langle f'; i', M'|e\Phi|f; i, M\rangle|^2 J_T(N), \tag{7}$$

where N_i is the degeneracy degree of the initial state i, M and M' enumerate the degenerate states of levels i and i', and final and initial energies are related through

$$E_i' \simeq E_i - \Delta_{ff'} - N\hbar\omega_{\mathrm{ph}}. \tag{8}$$

Following the Appendix, one finally gets for the probability of excitation:

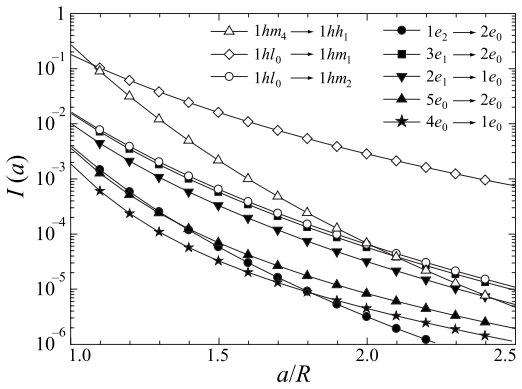

FIG. 10. Factors $I_{ii'}$ for erbium excitation/deexcitation by electron intraband transitions as a function of a/R, where a is the distance of the Er^{3+} ion from the center of the NC and R the radius of the NC.

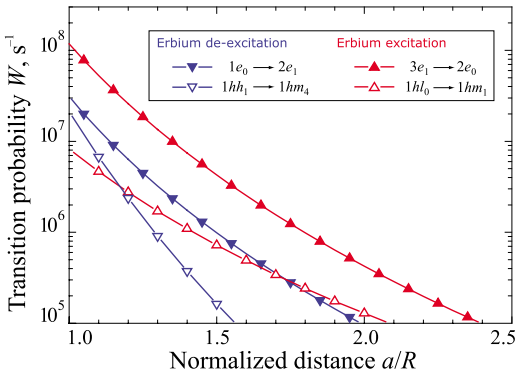

FIG. 11. (Color online) The probability of the most effective excitation and deexcitation processes as a function of a/R (a is the erbium distance from the center of a NC and R the radius of the NC) for a NC with diameter 3.1 nm.

$$W_{i'i} = \frac{\pi}{2\sqrt{\varepsilon_2}} \frac{1}{\tau_{\rm rad}} \frac{1}{R^4} \left(\frac{\hbar c}{\Delta_{ff'}} \right)^3 \frac{e^2}{\varepsilon_2^2 \Delta_E} I_{i'i}(a) J_T(N), \qquad (9)$$

where ε_2 is the high-frequency dielectric constant in SiO_2 (as the energies transmitted are much larger than the phonon energies[26]), $\tau_{\rm rad}$ is the radiative lifetime of the erbium ion in the first-excited state ($^4I_{13/2}$), R is the radius of the NC, and $I_{i'i}(a)$ are dimensionless factors defined in the Appendix. From Eq. (9) one gets, by using values $\tau_{\rm rad}=2$ ms and $R=1.55$ nm:

$$W_{i'i} = 8.3 \times 10^9 \left(\frac{1.55 \text{ nm}}{R} \right)^4 I_{i'i}(a) J_T(N) \text{s}^{-1}. \qquad (10)$$

It has been shown that $I_{i'i}(a)$ are actually functions of the relation a/R for holes. In the case of electrons, there is only a weak additional dependence on the NC size, which one can neglect at least in the NC size range under consideration.[29] The results of calculations of the factors $I_{i'i}(a)$ for electrons and holes are presented in Fig. 10.

The energy required to get the Er^{3+} ion into the first-excited state $^4I_{13/2}$ (0.81 eV) with reasonable excess or shortage of energy can be covered by emission or absorption of phonons. The parameters of the multiphonon transition accompanying the Auger processes are not well defined. There is no data on existence of the electron-phonon interaction for Er^{3+} ions in the state $^4I_{13/2}$ in SiO_2. Thus, the interaction of confined carriers with optical phonons should be considered. The dispersion of optical phonons in bulk silicon can be neglected and the multimode model of the phonon transition becomes equivalent to the one-mode Huang-Rhys model.[26] Phonon factor $J_T(N)$ calculated for phonon energy equal to 60 meV (which is about the optical phonon energy in Si) is presented in Table I, calculated with a reasonable value of the Huang-Rhys parameter $S=0.1$ at room temperature. The exact value of the phonon energy and Huang-Rhys factor S are not known for the material considered here. We have used value $S=0.1$, which is in accordance with experimental values obtained for Er ions fluorozirconate glasses.[30] The influence of the value of Huang-Rhys parameter is shortly discussed in Ref. 31. The interaction with optical phonons is forbidden for electrons in silicon. One can suppose that the interaction of confined carriers with oxygen vibration could be also responsible for multiphonon assisted Auger processes in the system under consideration. The values of phonon factor $J_T(N)$ at $\hbar\omega_{\rm ph}=140$ meV corresponding to the oxygen vibrations are shown in Table I as well.

In Fig. 9 the most effective excitation processes for NCs with diameter 3.1 nm are demonstrated. The calculated values of the probabilities for these processes, as a function of the distance between a Er^{3+} ion and the nearest NC, are presented in Fig. 11.

B. Deexcitation of erbium by carriers confined in NCs

When considering erbium deexcitation due to intraband transitions of confined carriers, one can use the same formulas from Sec. IV A (and Appendix) except for interchanging initial and final states, as well as adjusting the phonon factor $J_T(N)$. If erbium excitation process takes place with carrier transition energy larger than $\Delta_{ff'}=0.81$ eV, and requires N phonons to be emitted, then the reverse process will be described by $J_T(-N)$ factor, which is much less than $J_T(N)$. That is why most of the processes appear either in excitation or in deexcitation section.

TABLE I. Phonon factor $J_T(N)$ calculated with $S=0.1$ for two different phonon energies $\hbar\omega_{\rm ph}$ and temperature $T=300$ K.

N	−2	−1	0	+1	+2	+3	+4	+5
$\hbar\omega_{\rm ph}=60$ meV	5.2×10^{-5}	0.0096	0.87	0.098	0.0054	0.2×10^{-3}	5.5×10^{-6}	1.2×10^{-7}
$\hbar\omega_{\rm ph}=140$ meV	9.0×10^{-8}	0.0004	0.9	0.091	0.0046	0.15×10^{-6}	3.8×10^{-3}	7.7×10^{-8}

The difference is not in the factor only. One should also take into account that the transitions under consideration take place between degenerate states. So the total probability is achieved by summation over the final states and averaging over the initial ones. As the degeneracy degree can be different for initial and final states, the probability of excitation and deexcitation processes can be different even for those of them that do not need phonons. This difference might be considerable for confined carriers, especially for holes. Since most of upper levels are described by larger values of moment F, having greater degeneracy degree, the probability of erbium deexcitation should be higher for the processes that do not require any phonons to be emitted or absorbed.

The most effective deexcitation processes for NCs with diameter 3.1 nm are demonstrated in Fig. 9 and calculated values are shown in Fig. 11.

C. Erbium excitation by the recombination of confined carriers

Let us consider the excitation of Er^{3+} ions by recombination of confined electron and hole. For the NCs under consideration ($d \sim 3.1$ nm), the recombination energy is larger than 1.5 eV. Therefore the energy transfer to the Er^{3+} ion by an Auger recombination of such an exciton can be effective only if it causes the direct transition of the ion into the third-excited state $^4I_{9/2}$ (energy of transition from the ground state $^4I_{15/2}$ is $\Delta_{03}=1.55$ eV), the fourth $^4I_{9/2}$ (transition energy $\Delta_{04}=1.9$ eV), or higher excited states. One should notice that the Er^{3+} ion can practically not be excited directly into the state $^4I_{13/2}$ via such a process, as it should be accompanied by multiphonon emission with the number of phonons $N \geq 5$. The phonon factor $J_T(N)$ is in this case very small (see Table I). In order to calculate the transition probability, we can use formula (3) if we assume that initial and final states of confined carriers now belong to different bands, and dividing the probability by the degeneracy of the final state since only one final state is empty if there is one-electron-hole pair in the NC. One should also choose appropriate parameters for the phonon system.

Crucial for the matrix element evaluation is to keep in mind that the value $\hbar\Delta k$ of momentum transmitted during recombination process is large. The minima of the conduction band in k space are shifted from the Γ point by the wave vector $k_0=0.85k_X$ (k_X is the Brillouin-zone edge). And it was shown in Ref. 32 that the momentum needed to transmit is even larger than $\hbar k_0$: $\hbar\Delta k=1.15\hbar k_X$. Such a great momentum can only be transferred to the f shell of the erbium ion by the Coulomb interaction at a distance that is less than the lattice constant of silicon. So the interaction has a contact character, and is determined by the electron and hole wave-function values at the position $\mathbf{a}$ of the erbium.

Once carriers are strongly confined in the NC and the tunneling is weak, the interaction is possible either inside the NC or in its vicinity. When dealing with the Coulomb interaction at distances smaller than the lattice constant, no screening should be taken into account any more and the effective dielectric constant value can be assumed to be $\varepsilon_{\text{eff}}=1$.[26,32] In this case the absolute value square of the matrix element in Eq. (3), averaged over the degenerate electron and hole states, can be calculated in analogy to bulk Auger processes[33,34] as

$$\overline{|\langle f',i'|e\Phi|f,i\rangle|^2} = \frac{(2\pi)^2 e^4}{\varepsilon_{\text{eff}}^2}|\langle f|z^2|f'\rangle|^2|\langle u_0|u_{cz}\rangle|^2|\xi^{e,i}(\mathbf{a})|^2 \times \frac{1}{N_{i'}}\sum_{M'}|\xi^{h,i'}_{M'0}(\mathbf{a})|^2, \tag{11}$$

where $\xi^{e,i}(\mathbf{r})$ is the electron envelope function in the initial state, and for shortness of notations, the total hole wave function in the final state is written as $\psi^{h,i'}_{FM}(\mathbf{r}) = \Sigma_m \xi^{h,i'}_{Mm}(\mathbf{r})u_m$ with u_m $(m=-1,0,+1)$ being the hole Bloch functions, $N_{i'}=2F'+1$ is the degeneracy of the hole state, $|\langle u_0|u_{cz}\rangle| \approx 0.25$ is the overlap integral between the bottom of the valence band $\Gamma^l_{25'}$, and the second conduction band $\Delta^c_{2'}$ with k at the position in the first Brillouin zone where the first conduction band has its minimum.[35] We remark that the quadrupole term plays here the main role in Coulomb interaction. Using expression (11) for the right-hand side of Eq. (7) divided by $N_{i'}$, we get the expression for the transfer probability for a given position of Er^{3+} and radius of the NC,

$$W_{\text{tr}}(\mathbf{a};R) = \frac{3\pi}{2}\frac{1}{\hbar\Delta_E}\left(\frac{e^2}{\varepsilon_{\text{eff}}R}\right)^2 Q(\mathbf{a};R)|\langle u_0|u_{cz}\rangle|^2\frac{\gamma_f r_f^4}{R^4}J_T(N). \tag{12}$$

Here the factor $\gamma_f r_f^4$ comes from the summation over f and averaging over f' of the absolute value square of the matrix element $\langle f|z^2|f'\rangle$, where $r_f \approx 0.43$ Å is the radius of the $4f$ shell of the Er^{3+} ion and the unknown factor γ_f is of the order of one. We have introduced a dimensionless factor $Q(\mathbf{a};R)$ defined by

$$Q(\mathbf{a};R) = \left(\frac{4\pi}{3}R^3\right)^2|\xi^{e,i}(\mathbf{a})|^2\frac{3}{N_{i'}}\sum_{M'}|\xi^{h,i'}_{M'0}(\mathbf{a})|^2. \tag{13}$$

If we assume the homogeneous probability distribution for the Er^{3+} ion inside the NC, then the probability of excitation transfer averaged over the position of the Er^{3+} ion inside the NC is given by Eq. (12) where, in place of $Q(\mathbf{a};R)$, we have

$$Q_{\text{in}}(R) = \frac{1}{\frac{4\pi}{3}R^3}\int_{a<R} d^3\mathbf{a}Q(\mathbf{a};R). \tag{14}$$

In order to calculate the average transfer probability at some distance D from the NC boundary, we introduce

$$Q_{\text{surf}}(R) = \frac{1}{4\pi}\int d\Omega Q(\mathbf{R};R), \tag{15}$$

where the integral is taken over the full solid angle Ω. Then the above-mentioned probability is given by Eq. (12) where, in place of $Q(\mathbf{a};R)$, we have

$$Q_{\text{surf}}(R)\exp[-2(\tilde{\kappa}_e+\tilde{\kappa}_h)D/R]. \tag{16}$$

Here the dimensionless factors

TABLE II. Calculated parameters of several interband transitions for NC diameter of 3.1 nm.

Transition	$E_{i'i}-\Delta_{03}$ (meV)	$E_{i'i}-\Delta_{04}$ (meV)	Q_{in}	Q_{surf}	$2(\tilde{\kappa}_e+\tilde{\kappa}_h)$
$1e_0 \rightarrow 1hm_1$	−41	−391	1.34	0.043	98.9
$2e_0 \rightarrow 1hm_1$	186	−164	1.24	0.098	98.0
$1e_0 \rightarrow 1hh_1$	128	−222	1.06	0.19	97.7
$2e_0 \rightarrow 1hh_1$	327	−23	0.77	0.20	96.8

$$\tilde{\kappa}_{e(h)} = \sqrt{\frac{2m^{\text{o}}_{e(h)}[U_{e(h)} - E_{e(h)}]R^2}{\hbar^2}} \tag{17}$$

determine the decay of the electron and hole wave functions outside the NC, E_e and E_h are the electron and hole quantization energies, m^{o}_e and m^{o}_h are the electron and hole masses outside the NC, and U_e=3.2 eV and U_h=4.3 eV are the corresponding energy barriers at the NC boundary. For the considered NCs, $2(\tilde{\kappa}_e+\tilde{\kappa}_h)$ is on the order of 10^2 (see Table II). Therefore the probability of the excitation transfer by the electron-hole recombination decays rapidly with increase in the distance between the erbium and NC. It becomes negligible at the distance of only several angstroms.

For local vibrations of erbium ions in fluorozirconate glass by optical transitions from the higher excited states into the ground state, the values around $\hbar\omega_{\text{ph}}$=60 meV and S=0.1 were reported in Ref. 30. We note that bulk optical phonons in Si also have approximately the same energy. These values we have used for the calculation of the phonon factor $J_T(N)$ in the transfer probability (see Table I). For the estimation of the transfer probability, we have also used γ_f=1. Then Eq. (12) can be written as

$$W_{\text{tr}} = 0.8 \times 10^{11} Q J_T(N) \ \text{s}^{-1}. \tag{18}$$

We have analyzed transitions induced by electron and holes, being in one of the two lowest states. The numerical factors Q_{in} and Q_{surf} are given in Table II for R=1.55 nm together with the corresponding energies, which should be compensated by phonons and the decay factor $2(\tilde{\kappa}_e+\tilde{\kappa}_h)$.

From the data presented in Table II and using Table I, and Eqs. (16) and (18), one can see that the electron-hole recombination can effectively excite an Er^{3+} ion situated inside the NC or at a very short distance from its boundary in a nanosecond or even shorter time scale. However, this ultrafast excitation process does not lead to an immediate excitation of the first $^4I_{13/2}$ excited state of the Er^{3+} ion relevant for the 1.55 μm emission. Transition to this state can occur only via a subsequent multiphonon relaxation process, which takes place on a microsecond time scale.

D. Dipole-dipole contribution for the interband transitions

When an erbium ion is situated at a distance $a \gg R$, one can expand the Coulomb interaction between the recombining electron-hole pair in the NC and the erbium ion in SiO_2 into the series over the coordinate of the confined carrier. In the leading order, such an approximation results into the dipole-dipole interaction, being the reason for the so-called Förster mechanism of excitation.[10] In this case, the large excess momentum of the confined pair is transferred to the boundary of the NC in the process of recombination or the recombination is accompanied by emission of a phonon as in the radiative exciton recombination.[22]

The probability of the excitation governed by the dipole-dipole interaction can be presented as

$$W_{\text{dd}} = \frac{8\pi}{3}\frac{1}{\hbar^2\omega_{\text{ph}}}\frac{e^4}{\varepsilon^2_{\text{eff}}a^6}d^2_{\text{ex}}\sum_{j\geq 3} d^2_{0j}J_T(N_j), \tag{19}$$

where $J_T(N_j)$ is the phonon factor and d_{ex} is the dipole momentum of the confined exciton, which can be estimated by using its relation to the confined exciton radiative lifetime,

$$\frac{1}{\tau^{\text{rad}}_{\text{ex}}} = \frac{4e^2E^3_{\text{ex}}d^2_{\text{ex}}n_{\text{eff}}}{3\hbar^4c^3}. \tag{20}$$

Here E_{ex} is the exciton energy and the effective refraction index n_{eff} is determined by the formula from Ref. 36

$$n_{\text{eff}} = \left(\frac{\varepsilon_{\text{m}}}{\varepsilon_{\text{eff}}}\right)^2 \varepsilon_{\text{m}}{}^{1/2}, \tag{21}$$

where ε_{Si} and ε_{m} are the dielectric constants of silicon and medium, respectively, and $\varepsilon_{\text{eff}}=(\varepsilon_{\text{Si}}+2\varepsilon_{\text{m}})/3$.

Matrix elements d_{0j} in Eq. (19) correspond to the transitions in the f shell of Er^{+3} and can be expressed via the corresponding oscillator strengths P_{0j}:

$$d^2_{0j} = \frac{3\hbar^2}{2m_0\Delta_{0j}n_{\text{m}}}P_{0j}, \tag{22}$$

where, in the simplest approximation, n_{m} is the refraction index of the medium.[37] To our knowledge, there is no data in the literature concerning the oscillator strengths of transitions between the levels of the Er^{3+} ion in the considered inhomogeneous media. However, we can estimate them via the oscillator strengths found for several glasses and solutions:[37,38] $P_{03}=1-3\times10^{-7}$ for transition $^4I_{9/2}\rightarrow{}^4I_{15/2}$, and $P_{04}\approx 2\times10^{-6}$ for transition $^4I_{9/2}\rightarrow{}^4I_{15/2}$. Based on these data, we estimate $d^2_{03}=1\times10^{-22}$ cm^2, and $d^2_{04}=7\times10^{-22}$ cm^2.

The calculation leads to the estimation

$$W_{\text{dd}} \lesssim 10^{-1}\left(\frac{R}{a}\right)^6\frac{1}{\tau^{\text{rad}}_{\text{ex}}}. \tag{23}$$

Thus, one can see that the Förster mechanism does not work effectively for the considered system, especially at some distance from the NC, because the radiative recombination of confined carriers is a faster process. Again the excitation of

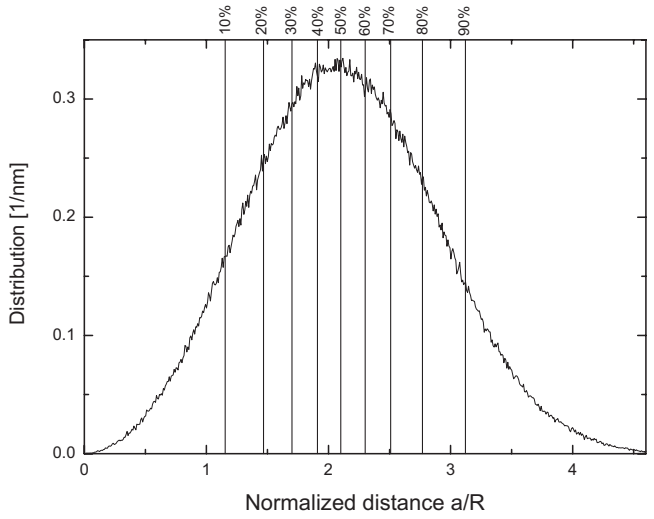

FIG. 12. A simulation of the distance distribution of Er^{3+} ions to the center of their nearest neighboring NC, assuming a random distribution of both: 6.6% of the Er^{3+} ions are contained inside NCs.

the first-excited state of the Er^{3+} is additionally delayed by the multiphonon relaxation from the higher excited states.

V. DISCUSSION

In the previous section we have shown that the Si-NC mediated excitation of Er^{3+} ions can proceed by a variety of physical processes. For all of these, efficiency depends on the distance between Si-NC and Er. Therefore we have generated a simulation of the Er^{3+} distribution as a function of the distance from the nearest Si NC (see Fig. 12) based on sample characteristics (Er and NC concentrations, and NC size), assuming a random distribution of both Si NCs and Er^{3+} ions in the SiO_2 matrix. As can be seen, the vast majority of the Er^{3+} content is positioned outside the NCs with only 6.6% of the Er^{3+} contained inside the NCs volume. In addition to this statistical prediction, we note that during crystallization process,[2] a considerable part of the Er^{3+} ions statistically present inside the NCs will become trapped at the Si NC/ SiO_2 boundary. These Er^{3+} ions are susceptible to an instantaneous excitation directly into the first-excited state via direct absorption of photons with enough energy to excite erbium and create an electron-hole pair in the NC. In silicon the absorption processes are usually accompanied by phonon emission due to indirect band structure. When an Er^{3+} ion is located inside a NC, the absorption can be accompanied by an excitation of this ion instead of phonon emission. This process is not considered in the theoretical part of this paper. We also note that the Er^{3+} ions remaining in the NC will induce a donor center, as a result of which they will deexcite nonradiatively very fast.[32]

As we can see from Fig. 4 in panel **b**, the fast excitation of Er^{3+} ions is completed within 20 ns after the excitation pulse and we have estimated in our previous contribution[21] that ~50% of the Er^{3+} content is involved in this fast process. The observed fast (submicrosecond) Er-related PL is only possible when Er^{3+} is excited directly into the first-excited state $^4I_{13/2}$. From Fig. 12 one can see that approximately 10% of Er^{3+} ions occur at a distance that is less than 1.15R from the NCs' centers, where according to Fig. 11, the most effective carrier cooling processes can provide Er^{3+} excitation at times shorter than 20 ns. However, we should point out that the presented calculations of transition probabilities serve mostly as a demonstration that such a fast mechanism is physically feasible. The theoretical considerations are valid for a single hole/single electron transition and for strictly spherical Si quantum dots. In this case, strong selection rules appear and only matrix elements of some higher multipoles of the electric-field potential lead to considerable nonvanishing contributions, causing a strong decrease in the probability with increasing distance from Er^{3+} to Si NCs. For example, the Auger process accompanied by the $3e_1 \rightarrow 2e_0$ transition is dominated by the quadrupole-dipole interaction (the dipole is related to Er^{3+}). Therefore one expects that the real probabilities might be higher than the calculated ones and will decrease less abruptly with distance due to nonsphericity of Si NCs. Even more important is the possibility of multiple exciton generation in a single NC, also not accounted for in the calculations. Under the excitation conditions used in the experiment, we estimate that, on average, about five electron-hole pairs are created per Si NC. On one side it will directly increase the excitation probability of Er^{3+} by a given NC at the initial stage. On the other side the strong exciton-exciton interaction will then generate very hot carriers, leading to population of higher excited states whose participation has not been considered in Sec. IV. This will result in much higher transfer rates due to a higher electron state localization outside Si NC. All these effects will contribute to the fast PL and improve the agreement with our experimental results.

Previously, in Ref. 21, we have estimated that ~0.5% of the total Er^{3+} decay radiatively ($\tau \sim 3$ ms) after excitation. From these 0.5% of ions, ~50% have been excited due to the fast process but have not been deexcited by the inverse mechanism: the "residual concentration." The other ~50% (~0.25% of the total Er^{3+} content in the sample) have been excited due to interband recombination of the carriers in the NC. In our theoretical considerations, we have shown that the excitation via the Auger process, accompanied by recombination of an exciton in the Si NC, can only take place via the contact. The Förster mechanism is not effective as shown in Sec. IV C. In any case the excitation of Er^{3+} ion accompanied by a recombination of an electron-hole pair takes place into the second or the third-excited state of the $4f$ shell of Er^{3+}. The characteristic excitation of the 1.5 μm Er^{3+} PL is, in this case, a two-step process with time constant $\tau = \tau_1 + \tau_2$, where τ_1 is the characteristic Er excitation into one of the higher excited states by the band-to-band recombination of confined carriers on the nanosecond or even shorter time scale and $\tau_2 \approx 1.2$ μs is the relaxation time of the excited Er^{3+} from a higher into the first-excited state $^4I_{13/2}$. This process is responsible for the microsecond rise of the Er-related PL signal.

Following the described model, one expects that the fast-to-slow Er^{3+} PL ratio will depend on the number of hot carriers confined in the Si NCs: a high number of hot carriers will favor the fast intraband excitation process and thus in-

crease the relative importance of the fast Er^{3+} PL. This is indeed confirmed in Fig. 5, where we can see that under excitation conditions where creation of "hot" carriers is more likely, i.e., excitation with higher energy photons or high-flux pumping and subsequent multiple carrier generation in the NCs, the fast-to-slow PL intensity ratio of Er PL increases. In the case of formation of several electron-hole pairs per Si NC, these can undergo a quick Auger recombination process and in that way the excess pairs escape from participating in the slow excitation transfer process.

Therefore, the following sequence of excitation and deexcitation processes can be proposed: (1) After the laser pulse, an Auger-like process of fast excitation takes place by intraband relaxation of hot carriers, transferring their excess energy directly into the first-excited state of Er^{3+} ion. Up to $\sim$50% of all the Er^{3+} content is in the effective range of this interaction before the deexcitation processes start to decrease the number of excited ions. We note that this percentage is dependent on the erbium concentration as indeed observed experimentally in Ref. 39. (2) Fast deexcitation of Er^{3+} takes place by a reverse process, transferring energy to carriers confined in the NCs. This process must be phonon assisted when the involved transitions do not match the energy conservation requirements, which will manifest in a slower PL decay and temperature dependence of the characteristic decay constant. The hot carriers in the NCs undergo an intraband relaxation accompanied by phonon emission, which reduces the number of carriers available for the "quick" excitation process. The rate of relaxation processes should increase with temperature. A small percentage of the excited Er^{3+} ions will overcome the fast deexcitation, giving rise to the residual concentration of Er^{3+}, which is excited in the nanoseconds time window and deexcites radiatively. This is revealed in the Er^{3+} PL kinetics as the nonzero origin of the microsecond rise and subsequent radiative decay of Er^{3+} PL. (3) Once the confined carriers have cooled down to the bottom (top) of the conduction (valence) band, there is a probability of Er^{3+} excitation by recombination to the upper Er excited states, as described above. This probability exists also on shorter time scales but the number of Er^{3+} ions that can be accessed is low and therefore this interband process is covered by the intraband excitation process.

Based on the presented experimental data and theoretical modeling, we conclude that three types of optically active Er^{3+} ions coexist in the investigated material: Type 1; Er^{3+} ions that can only be excited resonantly under direct excitation. These ions have predominantly radiative decay—like Er^{3+} in SiO_2—and are at large enough distance from the Si NCs to prevent their interaction. Type 2; Er^{3+} ions that are excited by energy transfer from interband recombination of excitons in Si NCs at the microseconds time regime and which decay predominantly radiatively ($\tau \sim 2-3$ ms) independent of temperature. These type of Er^{3+} ions are those accounted for in the usual estimations of optical activity measurements and constitute about 0.25–0.5% of the total Er^{3+} content. Type 3; Er^{3+} ions excited via the intraband transition of carriers in the NCs and with very strong nonradiative quenching, responsible for the submicrosecond PL described above, whose properties mirror those of Er^{3+} in crystalline Si ($\sim$50% of Er^{3+}). A small percentage of these ions will overcome the fast nonradiative deexcitation and will be also accounted for in optical activity measurements.

Finally, for the sake of completeness we note that in addition to these, there could also be Er dopants that are not optically active due to, e.g., precipitation.

An independent confirmation of the proposed excitation model of Er^{3+} ions by intraband transitions of confined carriers in the Si NC is indeed given by Fig. 8. There, for excitation energy higher than $E_{th} \approx 2.6-2.7$ eV, a second excitation mechanism (due to intraband carrier cooling) is enabled, increasing the ratio between absorption and effective excitation cross section of Er PL. This threshold energy is sufficient to create a hot carrier that can excite Er^{3+} directly into the first-excited state by cooling into the bottom of the conduction band (or the top of the valence band).[40]

VI. CONCLUSIONS

With the results of this study, an important puzzle concerning the mechanism of the excitation of Er^{3+} by Si-NCs has been solved. We have shown that the "missing" dopants that were apparently losing optical activity upon doping with Si-NCs, and which did not contribute to PL, are actually very efficiently excited by the Si-NCs via an intraband Auger transfer process but undergo also a very effective excitation back-transfer process. The back-transferred carriers can again excite the Er^{3+} ion or escape from being available for the intraband excitation process due to thermalization and Auger recombination processes inside a NC. In particular, we point out that the results of this study clearly show that in the first microsecond after the excitation laser pulse, a vast majority of Er dopants attain the excited state, which implies that in that short-time window the population inversion is reached, and in that way fulfills a necessary, although in itself insufficient, condition for realization of optical gain and laser. Future research will tell whether the SiO_2:(Er, Si-NCs) material can be engineered in such a way that the sensitization of Er emission is realized without the detrimental effect of reduction in the concentration of Er^{3+} ions with the temperature-stable, predominantly radiative recombination. This study shows that to achieve it will require careful and simultaneous optimization of Er^{3+} and NC concentrations, NC size and size distribution, and, very importantly, very precise tuning of Er-NC distance on a nanometer scale.

On the other hand, we point out that fast recombination kinetics reported here leads to the effective recombination rate of Er^{3+} in the environment of Si-NCs, exceeding by two orders of magnitude the fastest quenching rate (due to the Auger process involving free carriers) reported for Er in crystalline Si. This very efficient PL quenching of Er-related PL might be explored for gigahertz modulation of the 1.5 μm emission from Er-doped structures.

APPENDIX: CALCULATIONS FOR THE EXCITATION DUE TO INTRABAND TRANSITION

When dealing with the Coulomb interaction between an f electron of an Er^{3+} ion situated in SiO_2 and a carrier confined in Si NC, one should take into account the difference in

dielectric constant values of Si ($\varepsilon_1=12$) and SiO_2 ($\varepsilon_2=2$). We note that the Auger process is determined by the high-frequency dielectric constant as the transition energy $\Delta_{ff'}$ is much larger than the lattice vibration energy.[26]

The potential created by a point charge q at the distance $\mathbf{a}$ from the center of the sphere of radius R ($R<a$) with dielectric constant ε_1 in the media with dielectric constant ε_2 is obtained as a solution to the Poisson equation and is given by the equations:

$$\Phi_1(\mathbf{r},\mathbf{a}) = \frac{q}{\varepsilon_2 a}\left[1+\sum_{l=1}^{\infty}\left(\frac{r}{a}\right)^l \frac{(2l+1)\varepsilon_2}{l\varepsilon_1+(l+1)\varepsilon_2}P_l(\cos\vartheta)\right], \tag{A1}$$

inside the sphere ($r<R$), and

$$\Phi_2(\mathbf{r},\mathbf{a}) = \frac{q}{\varepsilon_2|\mathbf{r}-\mathbf{a}|} - \frac{q(\varepsilon_1-\varepsilon_2)}{\varepsilon_2 r} \times\sum_{l=1}^{\infty}\left(\frac{R}{a}\right)^{l+1}\frac{l}{l\varepsilon_1+(l+1)\varepsilon_2}\left(\frac{R}{r}\right)^l P_l(\cos\vartheta), \tag{A2}$$

outside the sphere ($r>R$), where ϑ is the angle between $\mathbf{r}$ and $\mathbf{a}$: $\cos(\vartheta)=(\mathbf{r},\mathbf{a})/ra$. Note that the Coulomb potential in the case of interaction of two charges is given by $\frac{1}{2}[\Phi(\mathbf{r},\mathbf{a})+\Phi(\mathbf{a},\mathbf{r})]$, but it is easy to show that in our case $\Phi(\mathbf{r},\mathbf{a})=\Phi(\mathbf{a},\mathbf{r})$.

Let us consider the potential Φ in Eqs. (3) and (7). Introducing the coordinate $\mathbf{r}'$ related to the center of the ion ($r' \lesssim r_f$, where r_f is the size of the f shell) and using the fact that $r_f \ll a$, the potential can be expanded into a series by $\mathbf{r}'$, taking into account the linear term only:

$$\Phi(\mathbf{r},\mathbf{a}+\mathbf{r}') \approx \Phi(\mathbf{r},\mathbf{a}) + \frac{\partial\Phi(\mathbf{r},\mathbf{a})}{\partial\mathbf{a}}\mathbf{r}'. \tag{A3}$$

In order to use formulas (A1) and (A2), the integration of matrix elements in Eq. (7) should be produced over $\mathbf{r}'$ for $0<r'<r_f$. Relatively high energy barriers at the boundary of a NC (3.2 and 4.3 eV for electrons and holes, respectively) allow only a small portion of the confined carrier charge density to penetrate outside. The charge density of confined carriers occurring in SiO_2 due to tunneling is just a few percents.[22] Therefore the largest contribution is given by the Coulomb interaction induced by the carrier density inside the NC. To that end, it is enough to use potential Φ_1 (see Eq. (A1)) only. We can write for it

$$\frac{\partial\Phi_1(\mathbf{r},\mathbf{a})}{\partial\mathbf{a}} = \frac{q}{a^2\varepsilon_2}\mathbf{J}, \tag{A4}$$

where

$$\mathbf{J} = -\frac{\mathbf{a}}{a}J_1 + \frac{\mathbf{r}}{r}J_2, \tag{A5}$$

and

$$J_1 = 1+\sum_{l=1}^{\infty}\frac{(2l+1)\varepsilon_2}{l\varepsilon_1+(l+1)\varepsilon_2}\left(\frac{r}{a}\right)^l \times\left[(l+1)P_l(\cos\vartheta)+\cos\vartheta\frac{\partial P_l(\cos\vartheta)}{\partial\cos\vartheta}\right], \tag{A6}$$

$$J_2 = \sum_{l=1}^{\infty}\frac{(2l+1)\varepsilon_2}{l\varepsilon_1+(l+1)\varepsilon_2}\left(\frac{r}{a}\right)^l\frac{\partial P_l(\cos\vartheta)}{\partial\cos\vartheta}. \tag{A7}$$

Then Eq. (7) transforms into

$$W_{i'i} = \frac{2\pi e^4}{\hbar\Delta_E\varepsilon_2^2 a^4}\frac{1}{N_i}\sum_{M,M'}\frac{1}{N_f}\sum_{ff'}|\mathbf{d}_{ff'}\langle i',M'|\mathbf{J}|i,M\rangle|^2 J_T(N), \tag{A8}$$

where the ion dipole momentum is given by

$$\mathbf{d}_{ff'} = \int \psi_{f'}^*(\mathbf{r})\mathbf{r}\psi_f(\mathbf{r})\mathrm{d}^3\mathbf{r}. \tag{A9}$$

Averaging Eq. (A8) over the directions of $\mathbf{d}_{ff'}$, one gets

$$W_{i'i} = \frac{2\pi e^4}{3\varepsilon_2^2\hbar\Delta_E R^4}\frac{1}{N_f}\sum_{ff'}|\mathbf{d}_{ff'}|^2 I_{i'i}(a)J_T(N), \tag{A10}$$

where the dimensionless factor $I_{i'i}(a)$ is defined by

$$I_{i'i}(a) = \frac{1}{N_i}\left(\frac{R}{a}\right)^4\sum_{M,M'}|\langle i',M'|\mathbf{J}|i,M\rangle|^2, \tag{A11}$$

where the square of the matrix element absolute value is assumed to be averaged over the directions of vector a. Introducing the radiative lifetime τ_{rad} of the erbium ion in the first-excited state ($^4I_{13/2}$) (Ref. 41)

$$\frac{1}{\tau_{\mathrm{rad}}} = \frac{1}{N_{f'}}\sum_{ff'}\frac{4}{3}e^2 d_{ff'}^2\frac{\sqrt{\varepsilon_2}(\Delta_{ff'})^3}{\hbar^4 c^3}, \tag{A12}$$

one gets finally Eq. (9). The results of calculations of the factors $I_{i'i}(a)$ for electrons and holes are given in Fig. 10.

For completeness, we consider the contribution of carrier density outside the dot to the probability of Er^{3+} excitation. The potential Φ_2, given by Eq. (A2), should be used outside the NC. We get

$$\frac{\partial\Phi_2(\mathbf{r},\mathbf{a})}{\partial\mathbf{a}} = \frac{q}{R^2\varepsilon_2}\mathbf{J}', \tag{A13}$$

where

$$\mathbf{J}' = \frac{\mathbf{a}R}{a^2}J_1' - \frac{\mathbf{r}R}{ar}J_2' + \frac{(\mathbf{r}-\mathbf{a})R^2}{|\mathbf{r}-\mathbf{a}|^3}, \tag{A14}$$

$$J_1' = \sum_{l=1}^{\infty}\frac{\varepsilon_1-\varepsilon_2}{l\varepsilon_1+(l+1)\varepsilon_2}\left(\frac{R}{a}\right)^{(l+1)}\left(\frac{R}{r}\right)^{(l+1)} \times\left[(l+1)P_l(\cos\vartheta)+\cos\vartheta\frac{\partial P_l(\cos\vartheta)}{\partial\cos\vartheta}\right], \tag{A15}$$

$$J_2' = \sum_{l=1}^{\infty} \frac{\varepsilon_1 - \varepsilon_2}{l\varepsilon_1 + (l+1)\varepsilon_2} \left(\frac{r}{a}\right)^l \frac{\partial P_l(\cos\vartheta)}{\partial \cos\vartheta} \quad . \qquad \text{(A16)}$$

Producing the calculations analogous to the ones described above for the carriers being inside the NC, one can find that the contribution of the confined carriers tunneling to the excitation probability is given by an expression similar to Eq. (A10). Our calculations have shown that the input is negligible.

*Currently at: Laboratoire Kastler Brossel, Départements de Physique et de Biologie, Ecole Normale Supérieure, 46 rue d'Ulm, Paris, France.

[1] A. J. Kenyon, P. F. Trwoga, M. Federighi, and C. W. Pitt, J. Phys.: Condens. Matter **6**, L319 (1994).

[2] M. Fujii, M. Yoshida, Y. Kanzawa, S. Hayashi, and K. Yamamoto, Appl. Phys. Lett. **71**, 1198 (1997).

[3] C. E. Chryssou, A. J. Kenyon, T. S. Iwayama, C. W. Pitt, and D. E. Hole, Appl. Phys. Lett. **75**, 2011 (1999).

[4] D. Pacifici, G. Franzò, F. Priolo, F. Iacona, and L. Dal Negro, Phys. Rev. B **67**, 245301 (2003).

[5] P. G. Kik, M. L. Brongersma, and A. Polman, Appl. Phys. Lett. **76**, 2325 (2000).

[6] D. Kovalev, H. Heckler, M. Ben-Chorin, G. Polisski, M. Schwartzkopff, and F. Koch, Phys. Rev. Lett. **81**, 2803 (1998).

[7] M. E. Castagna, S. Coffa, M. Monaco, L. Caristia, A. Messina, R. Mangano, and C. Bongiorno, Physica E (Amsterdam) **16**, 547 (2003).

[8] A. Nazarov, J. M. Sun, W. Skorupa, R. A. Yankov, I. N. Osiyuk, I. P. Tjagulskii, V. S. Lysenko, and T. Gebel, Appl. Phys. Lett. **86**, 151914 (2005).

[9] R. J. Walters, G. I. Bourianoff, and H. A. Atwater, Nat. Mater. **4**, 143 (2005).

[10] T. Förster, Ann. Phys. **2**, 55 (1948).

[11] M. J. A. de Dood, J. Knoester, A. Tip, and A. Polman, Phys. Rev. B **71**, 115102 (2005).

[12] V. M. Agranovich and M. D. Galanin, *Electronic Excitation Energy Transfer in Condensed Matter* (Elsevier, New York, 1982).

[13] X. L. Wu, Y. F. Mei, G. G. Siu, K. L. Wong, K. Moulding, M. J. Stokes, C. L. Fu, and X. M. Bao, Phys. Rev. Lett. **86**, 3000 (2001).

[14] R. A. Senter, C. Pantea, Y. Wang, H. Liu, T. W. Zerda, and J. L. Coffer, Phys. Rev. Lett. **93**, 175502 (2004).

[15] M. Fujii, K. Imakita, K. Watanabe, and S. Hayashi, J. Appl. Phys. **95**, 272 (2004).

[16] O. Savchyn, F. R. Ruhge, P. G. Kik, R. M. Todi, K. R. Coffey, H. Nukala, and H. Heinrich, Phys. Rev. B **76**, 195419 (2007).

[17] K. Imakita, M. Fujii, and S. Hayashi, Phys. Rev. B **71**, 193301 (2005).

[18] J. Lee, J. H. Shin, and N. Park, J. Lightwave Technol. **23**, 19 (2005).

[19] M. Wojdak, M. Klik, M. Forcales, O. B. Gusev, T. Gregorkiewicz, D. Pacifici, G. Franzò, F. Priolo, and F. Iacona, Phys. Rev. B **69**, 233315 (2004).

[20] P. G. Kik and A. Polman, J. Appl. Phys. **88**, 1992 (2000).

[21] I. Izeddin, A. S. Moskalenko, I. N. Yassievich, M. Fujii, and T. Gregorkiewicz, Phys. Rev. Lett. **97**, 207401 (2006).

[22] A. S. Moskalenko, J. Berakdar, A. A. Prokofiev, and I. N. Yassievich, Phys. Rev. B **76**, 085427 (2007).

[23] A. J. Kenyon, C. E. Chryssou, C. W. Pitt, T. Shimizu-Iwayama, D. E. Hole, N. Sharma, and J. Humphreys, J. Appl. Phys. **91**, 367 (2002).

[24] A. Schenk and G. Heiser, J. Appl. Phys. **81**, 7900 (1997).

[25] J. R. Chelikowsky and M. Schlueter, Phys. Rev. B **15**, 4020 (1977).

[26] V. N. Abakumov, V. I. Perel, and I. N. Yassievich, *Nonradiative Recombination in Semiconductors* (Elsevier, New York, 1991).

[27] E. Hendry, M. Koeberg, F. Wang, H. Zhang, C. de Mello Donegá, D. Vanmaekelbergh, and M. Bonn, Phys. Rev. Lett. **96**, 057408 (2006).

[28] B. K. Ridley, *Quantum Processes in Semiconductors* (Clarendon, Oxford, 1982).

[29] A. A. Prokofiev, A. S. Moskalenko, and I. N. Yassievich, Mater. Sci. Eng., B **146**, 121 (2008).

[30] M. D. Shinn, W. A. Sibley, M. G. Drexhage, and R. N. Brown, Phys. Rev. B **27**, 6635 (1983).

[31] A. A. Prokofiev, A. S. Moskalenko, and I. N. Yassievich, J. Lumin. **121**, 222 (2006).

[32] A. A. Prokofiev, I. N. Yassievich, H. Vrielinck, and T. Gregorkiewicz, Phys. Rev. B **72**, 045214 (2005).

[33] I. N. Yassievich and L. C. Kimerling, Semicond. Sci. Technol. **8**, 718 (1993).

[34] A. S. Moskalenko, I. N. Yassievich, M. Forcales, M. Klik, and T. Gregorkiewicz, Phys. Rev. B **70**, 155201 (2004).

[35] M. Cardona and F. H. Pollak, Phys. Rev. **142**, 530 (1966).

[36] A. Thranhardt, C. Ell, G. Khitrova, and H. M. Gibbs, Phys. Rev. B **65**, 035327 (2002).

[37] B. R. Judd, Phys. Rev. **127**, 750 (1962).

[38] W. J. Miniscalco, J. Lightwave Technol. **9**, 234 (1991).

[39] K. Imakita, M. Fujii, and S. Hayashi, Eur. Phys. J. D **34**, 161 (2005).

[40] D. Timmerman, I. Izeddin, P. Stallinga, I. N. Yassievich, and T. Gregorkiewicz, Nat. Photonics **2**, 105 (2008).

[41] A. Suchocki and J. M. Langer, Phys. Rev. B **39**, 7905 (1989).